Abstracta

Ano XII - N. 03

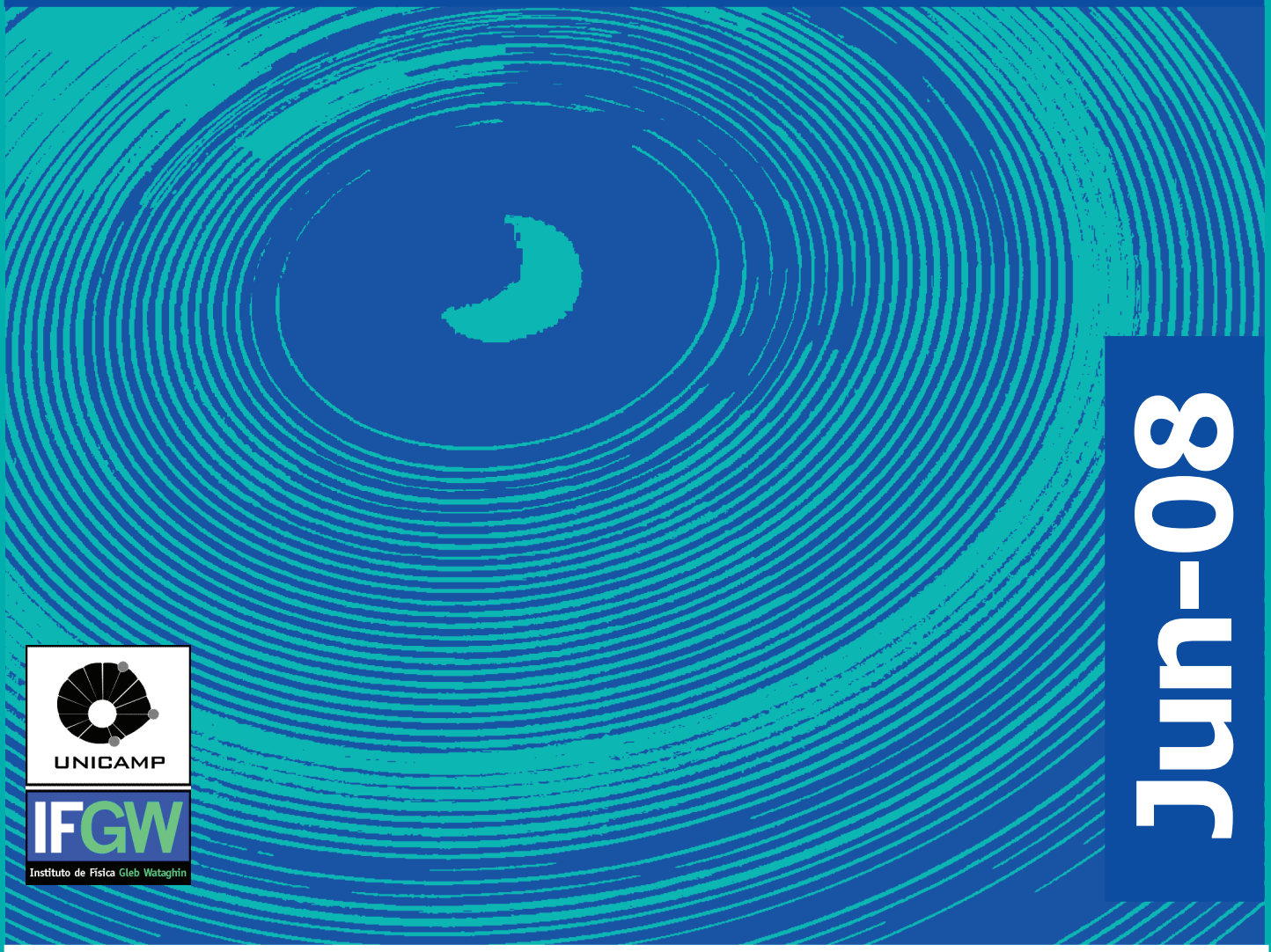

Jun-08

UNICAMP

IFGW

Instituto de Física Gleb Wataghin

Trabalhos Publicados

Maio 2008 à Junho 2008

P083-08 à P145 -08

Trabalhos Publicados

P083-08 "A new model to describe the crossover from superparamagnetic to blocked magnetic nanoparticles"

De Biasi, E., Zysler, R. D., Ramos, C. A., and Knobel, M.

A new model that considers the thermal probability of uniform magnetization inversion in magnetic nanoparticles is presented. We included the temporal window in consideration of the thermal average, which allowed us to take into account the hysteretic behavior, leading to a more clear description of the passage from one regime to another. From this formalism appears a superparamagnetic probability L that indicated the fraction of superparamagnetic particles we find on the ensemble at a given T, H and experimental time window. We have performed numerical simulations, including different time windows and considering the high- and low-temperature regimes. We compare our model with the analytic solution in zero and high- temperature limits and find that the proposed model agrees with the simulations. Measurements of fieldcooling and zero-filed-cooling magnetization as well as hysteresis loops were simulated applying this model, from which relevant considerations regarding the importance, applicability and limitations of this treatment could be obtained.

Journal of Magnetism and Magnetic Materials 320[14], E312-E315, 2008.

P084-08 "Application of Mossbauer spectroscopy to the study of corrosion resistance in NaCl solution of plasma nitrided AISI 316L stainless steel"

Olzon-Dionysio, M., de Souza, S. D., Basso, R. L. O., and de Souza, S.

Corrosion research in steels is one of the areas in which Mossbauer spectroscopy has become a required analytical technique, since it is a powerful tool for both identifying and quantifying distinctive phases (which contain Fe) with accuracy. In this manuscript, this technique was used to the study of corrosion resistance of plasma nitrided AISI 316L samples in the presence of chloride anions. Plasma nitriding has been carried out using dc glow-discharge, nitriding treatments, in medium of 80 vol.% H-2 and 20 vol.% N-2, at 673 K, and at different time intervals: 2, 4, and 7 h. Treated samples were characterized by means of phase composition and morphological analysis, and electrochemical tests in NaCl aerated solution in order to investigate the influence of treatment time on the microstructure and the corrosion resistance, proved by conversion electron Mossbauer spectroscopy (CEMS), glancing angle X-ray diffraction (GAXRD), scanning electron microscopy (SEM) and potentiodynamic polarization. A modified layer of about 8 gin was observed for all the nitrided samples, independently of the nitriding time. A metastable phase, S phase or gamma(N), was produced. It seems to be correlated with gamma'-Fe-4 N phase. If the gamma(N) fraction decreases, the gamma' fraction increases. The gamma(N) magnetic nature was analyzed. When the nitriding time increases, the results indicate that there is a significant reduction in the relative fraction of the magnetic gamma(N) (in) phase. In contrast, the paramagnetic gamma(N) (p) phase increases. The GAXRD analysis confirms the Mossbauer results, and it also indicates CrN traces for the sample nitrided for 7 h. Corrosion results demonstrate that time in the plasma nitriding treatment plays an important role for the corrosion resistance. The sample treated for 4 h showed the best result of corrosion resistance. It seems that the epsilon/gamma' fraction ratio plays an important role in thin corrosion resistance since this sample shows the maximum value for this ratio.

Surface & Coatings Technology 202[15], 3607-3614. 2008.

P085-08 "Charge ordering in amorphous WOx films"

Kopelevich, Y., da Silva, R. R., Rougier, A., and Luk'yanchuk, I. A.

We observed highly anisotropic viscous electronic conducting phase in amorphous WO1.55 films that occurs below a current (I)- and frequency (f)-dependent temperature T*(I,f). At T<T*(I,f) the rotational symmetry of randomly disordered electronic background is broken leading to the appearance of mutually perpendicular metallic- and insulating-like states. A rich dynamic behavior of the electronic matter occurring at T<T*(I,f) provides evidence for an interplay between pinning effects and electron-electron interactions. The results suggest a dynamic crystallization of the disordered electronic matter, viz. formation of sliding Wigner crystal, as well as the occurrence of quantum liquid-like crystal or stripe phase at low drives.

Physica B-Condensed Matter 403[5-9], 1211-1212, 2008.

P086-08 "Coercive field behavior of permalloy antidot arrays based on self-assembled template fabrication"

Pirota, K. R., Prieto, P., Neto, A. M. J., Sanz, J. M., Knobel, M., and Vazquez, M.

High-density magnetic antidot arrays have been fabricated by deposition of Fe20Ni80 thin films on self-assembled nanoporous alumina membranes (NAM) with high-order hexagonal symmetry. The magnetic properties induced by the size and the geometry configuration of the holes introduced in a Fe20Ni80 thin film are discussed based on hysteresis loops measured as a function of temperature. The precursor NAMs have pore diameters ranging between 35 and 95nm (55 and 75nm after the film deposition) and a lattice parameter of 105 nm. An enormous increase of coercitivity, as compared with the corresponding continuous films, was observed for temperatures between 2 and 300 K. This effect depends on the size and surface density of holes in the Fe20Ni80 antidot arrays. Rutherford backscattering spectrometry (RBS) measurements were performed in order to better clarify the magnetic material that was eventually deposited within the NAM pores.

Journal of Magnetism and Magnetic Materials 320[14], E235-E238, 2008.

P087-08 "Controlling phase space caustics in the semiclassical coherent state propagator"

Ribeiro, A. D. and de Aguiar, M. A. M.

The semiclassical formula for the quantum propagator in the coherent state representation < z ''vertical bar e(-i (H) over barT/h)vertical bar z'> is not free from the problem of caustics. These are singular points along the complex classical trajectories specified by z', z '' and T where the usual quadratic approximation fails, leading to divergences in the semiclassical formula. In this paper, we derive third order approximations for this propagator that remain finite in the vicinity of caustics. We use Maslov's method and the dual representation proposed in Phys. Rev. Lett. 95, 050405 (2005) to derive uniform, regular and transitional semiclassical approximations for coherent state propagator in systems with two degrees of freedom.

Annals of Physics 323[3], 654-672. 2008.

P088-08 "Correlation of the highest-energy cosmic rays with the positions of nearby active galactic nuclei"

Abraham, J., Abreu, P., Aglietta, M., Aguirre, C., Allard, D., Allekotte, I., Allen, J., Allison, et all

Data collected by the Pierre Auger Observatory provide evidence for anisotropy in the arrival directions of the cosmic rays with the highest-energies, which are correlated with the positions of relatively nearby active galactic nuclei (AGN) [Pierre Auger Collaboration, Science 318 (2007) 938]. The correlation has maximum significance for cosmic rays with energy greater than similar to 6 x 10(19) eV and AGN at a distance less than similar to 75 Mpc. We have confirmed the anisotropy at a confidence level of more than 99% through a test with parameters specified a priori, using an independent data set. The observed correlation is compatible with the hypothesis that cosmic rays with the highest-energies originate from extra-galactic sources close enough so that their flux is not significantly attenuated by interaction with the cosmic background radiation (the Greisen-Zatsepin-Kuz'min effect). The angular scale of the correlation observed is a few degrees, which suggests a predominantly light composition unless the magnetic fields are very weak outside the thin disk of our galaxy. Our present data do not identify AGN as the sources of cosmic rays unambiguously, and other candidate sources which are distributed as nearby AGN are not ruled out. We discuss the prospect of unequivocal identification of individual sources of the highest-energy cosmic rays within a few years of continued operation of the Pierre Auger Observatory.

Astroparticle Physics 29[3], 188-204. 2008.

P089-08 "Crystal structure and low temperature physical properties of Ho2CoGa8 intermetallic antiferromagnet"

Adriano, C., Mendonca-Ferreira, L., Bittar, E. M., and Pagliuso, P. G.

We have synthesized single crystalline samples of Ho2CoGa8 intermetallic compound using a Ga-flux method. This compound crystallizes with a tetragonal structure, space group P4/mmm, and lattice parameters a=4.219(5) angstrom and c=10.99(2) angstrom. This structure is a bilayer version of the HoCoGa5 (1-1-5) which hosts a series of heavy-fermion superconductors and complex antiferromagnetic intermetallic systems. Measurements of magnetic susceptibility, heat capacity, and electrical resistivity revealed that Ho2CoGa8 is a metallic Curie-Weiss paramagnet at high temperature and presents an antiferromagnetic ordering below T-N similar to 5 K. The low temperature magnetic properties of this compound show the effects of tetragonal crystalline electrical field and the Ruderman-Kittel-Kasuya-Yosid interactions and the results presented here are compared with a broader description of the evolution of the low-T magnetic properties of structurally related series of rare-earth based tetragonal 2-1-8 and 1-1-5 compounds.

Journal of Applied Physics 103[7]. 07B712. 2008.

P090-08 "Delay time computation for relativistic tunneling particles"

Bernardini, A. E.

We study the tunneling zone solutions of a one-dimensional electrostatic potential for the relativistic (Dirac to Klein-Gordon) wave equation when the incoming wave packet exhibits the possibility of being almost totally transmitted through the barrier. The transmission probabilities, the phase times and the dwell times for the proposed relativistic dynamics are obtained and the conditions for the occurrence of accelerated tunneling transmission are all quantified. We show that, in some limiting cases, the analytical difficulties that arise when the stationary phase method is employed for obtaining phase (traversal) tunneling times are all overcome. Lessons concerning the phenomenology of the relativistic tunneling suggest revealing insights into condensed-matter experiments using electrostatic barriers for which the accelerated tunneling effect can be observed.

European Physical Journal C 55[1], 125-132. 2008.

P091-08 "Denoising swallowing sound to improve the evaluator's qualitative analysis"

Spadotto, A. A., Papa, J. P., Gatto, A. R., Cola, P. C., Pereira, J. C., Guido, R. C., Schelp, A. O., Maciel, C. D., and Montagnoli, A. N.

Swallowing dynamics involves the coordination and interaction of several muscles and nerves which allow correct food transport from mouth to stomach without laryngotracheal penetration or aspiration. Clinical swallowing assessment depends on the evaluator's knowledge of anatomic structures and of neurophysiological processes involved in swallowing. Any alteration in those steps is denominated oropharyngeal dysphagia, which may have many causes, such as neurological or mechanical disorders. Videofluoroscopy of swallowing is presently considered to be the best exam to objectively assess the dynamics of swallowing, but the exam needs to be conducted under certain restrictions, due to patient's exposure to radiation, which limits periodical repetition for monitoring swallowing therapy. Another method, called cervical auscultation, is a promising new diagnostic tool for the assessment of swallowing disorders. The potential to diagnose dysphagia in a noninvasive manner by assessing the sounds of swallowing is a highly attractive option for the dysphagia clinician. Even so, the captured sound has an amount of noise, which can hamper the evaluator's decision. In that way, the present paper proposes the use of a filter to improve the quality of audible sound and facilitate the perception of examination. The wavelet denoising approach is used to decompose the noisy signal. The signal to noise ratio was evaluated to demonstrate the quantitative results of the proposed methodology.

Computers & Electrical Engineering 34[2], 148-153. 2008.

P092-08 "Determination of spin polarization in InAs/GaAs selfassembled quantum dots"

Hernandez, F. G. G., Alegre, T. P. M., and Medeiros-Ribeiro, G.

The spin polarization of electrons trapped in InAs self-assembled quantum dot ensembles is investigated. A statistical approach for the population of the spin levels allows one to infer the spin polarization from the measured values of the addition energies. From the magnetocapacitance spectroscopy data, the authors found a fully polarized ensemble of electronic spins above 10 T when B parallel to[001] and at 2.8 K. Finally, by including the gtensor anisotropy, the angular dependence of the spin polarization with the magnetic field B orientation and strength could be determined.

Applied Physics Letters 92[13]. 132106. 2008.

P093-08 "Direct and indirect exciton states in GaAs-(Ga, Al) As double quantum wells under crossed electric and magnetic fields"

Oliveira, L. E., de Dios-Leyva, M., and Duque, C. A.

A theoretical study of the direct and indirect exciton states in GaAs/Ga1-xAlxAs coupled double quantum wells under crossed electric and magnetic fields is presented. The setup of the system under consideration consists of an electric field perpendicular to the layers and an in-plane applied magnetic field. For calculations we use a variational procedure (by using a simple hydrogen-like envelope wave-function), in the

effective-mass and parabolic-band approximations. Present theoretical results are found in fair agreement with available experimental measurements in double quantum well heterostructures under applied electric and magnetic fields.

Microelectronics Journal 39[3-4], 398-401. 2008.

P094-08 "Effect of the Rashba and Dresselhaus spin-splitting terms on the electron g factor in semiconductor quantum wells under applied magnetic fields"

Bruno-Alfonso, A., Porras-Montenegro, N., Reyes-Gomez, E., and Oliveira, L. E.

We use the Ogg-McCombe Hamiltonian together with the Dresselhaus and Rashba spin-splitting terms to find the g factor of conduction electrons in GaAs-(Ga,Al)As semiconductor quantum wells (QWS) (either symmetric or asymmetric) under a magnetic field applied along the growth direction. The combined effects of non-parabolicity, anisotropy and spin-splitting terms are taken into account. Theoretical results are given as functions of the QW width and compared with available experimental data and previous theoretical works.

Physica E-Low-Dimensional Systems & Nanostructures 40[5], 1464-1466. 2008.

P095-08 "Effects of hydrostatic pressure and crossed electric and magnetic fields on shallow-donor states in GaAs/Ga1-xAlxAs quantum wells"

Tangarife, E., Lopez, S. Y., de Dios-Leyva, M., Oliveira, L. E., and Duque, C. A.

We have used a variational procedure within the envelopefunction and parabolic-band approximations to investigate the effects of hydrostatic pressure and crossed electric and magnetic fields on shallow-donor states in GaAs/Ga1-xAlxAs quantum wells. The donor variational envelope wave function is obtained through a hydrogenic 1s-like wave function and an expansion in a complete set of trigonometrical functions, and a detailed study is performed of the dependence of the donor binding energies on the applied hydrostatic pressure and applied in-growth direction electric and in-plane magnetic fields.

Microelectronics Journal 39[3-4], 431-434. 2008.

P096-08 "Eikonal zeros in the momentum transfer space fromproton-proton scattering: an empirical analysis"

Avila, R. F. and Menon, M. J. By means of improved empirical fits to the differential cross section data on pp elastic scattering at 19.4 <= root s <= 62.5 GeV and making use of a semi-analytical method, we determine the eikonal in the momentum transfer space (the inverse scattering problem). This method allows for the propagation of the uncertainties from the fit parameters up to the extracted eikonal, providing statistical evidence that the imaginary part of the eikonal (real part of the opacity function) presents a zero (change of signal) in the momentum space, at q(2) approximate to 7 +/- 1 GeV2. We discuss the implication of this change of signal in the phenomenological context, showing that eikonal models with one zero provide good descriptions of the differential cross sections in the full momentum transfer range, but that is not the case for models without zero. Empiricalconnections between the extracted eikonal and results from a Yang conjecture. In addition, we present a critical review on the pp differential cross section data presently available at high energies.

European Physical Journal C 54[4], 555-576. 2008.

P097-08 "Electron spin resonance of Gd3+ in GdmMnIn3m+2n (M=Rh,Ir; n=0,1; m=1,2) antiferromagnets"

Duque, J. G. S., Adriano, C., Lora-Serrano, R., Rettori, C., Urbano, R. R., Sarrao, J. L., Oseroff, S. B., and Pagliuso, P. G.

We report electron spin resonance experiments of Gd3+ in the GdmMnIn3m+2n (M=Rh,Ir; n=0,1; m=1,2) intermetallic compounds. For T > T-N similar to 45 K, all compounds present a single Dysonian resonance and show a Korringa-like temperature dependence of the linewidth, Delta H=a+bT. The residual linewidth a is strongly affected by the transition metal M=Rh or Ir and/or by the layering (m=1 or 2) or change in structure (n=0,1). The residual linewidth is associated with an unresolved crystalline electrical field (CEF) fine structure. Consequently, a systematic evolution of the CEF in the GdmMnIn3m+2n compounds is inferred. A discussion to what extent our results can explain to the CEF effects observed in isostructural R-based compounds will be given.

Journal of Applied Physics 103[7]. 07B733. 2008.

P098-08 "Enhanced strange baryon production in Au+Au collisions compared to p+p at root s(NN)=200 GeV"

Abelev, B. I., Aggarwal, M. M., Ahammed, Z., Anderson, B. D., Arkhipkin, D., Averichev, G. S., Bai, Y., et all

We report on the observed differences in production rates of strange and multistrange baryons in Au+Au collisions at s(NN)=200 GeV compared to p+p interactions at the same energy. The strange baryon yields in Au+Au collisions, when scaled down by the number of participating nucleons, are enhanced relative to those measured in p+p reactions. The enhancement observed increases with the strangeness content of the baryon, and it increases for all strange baryons with collision centrality. The enhancement is qualitatively similar to that observed at the lower collision energy s(NN)=17.3 GeV. The previous observations are for the bulk production, while at intermediate p(T),1 < p(T)< 4 GeV/c, the strange baryons even exceed binary scaling from p+p yields

Physical Review C 77[4]. 2008.

P099-08 "Entanglement induced by noise: Emitters in thermal bandgap reservoirs"

Mogilevtsev, D., Moreira, F., Cavalcanti, S. B., and Kilin, S.

Emitter-field interactions in a bandgap reservoir at a finite temperature are investigated by means of a time-local Lindblad master equation derived specifically for this purpose. It is demonstrated that the entangled field-emitter state that arises as a result of the interaction does not survive at finite temperatures. On the other hand, the probability to excite such an entangled state by thermal excitation is found to be close to unity.

Physica E-Low-Dimensional Systems & Nanostructures 40[6], 2141-2143. 2008.

P100-08 "Entanglement reciprocation using three level atoms in a lambda configuration"

Lourenco, F. C. and Vidiella-Barranco, A.

We propose a scheme in which entanglement can betransferred from atoms (discrete variables) to entangled states of cavity fields (continuous variables). The cavities play the role of a kind of quantum memory for entanglement, in such a way that it is possible to retrieve it back to the items. In our method, two three level atoms in a lambda, configuration, previously entangled, are set to interact with single mode cavity fields prepared in coherent states. During the process, one e-bit of entanglement may be deposited in the cavities in an efficient way. We also show that the stored entanglement may be transferred back to flying atoms.

European Physical Journal D 47[1], 127-131. 2008.

P101-08 "Evidence of mixed valence in (Eu1-xYbx)Ga-4 single crystals"

Loula, G. D., da Silva, L. M., dos Santos, A. O., Medina, A. N., and Gandra, F. G.

In this paper we report on the magnetization and specific heat results on single crystals of the series (Eu,Yb)Ga-4 aiming to study a possible valence change on both RE ions. The results show a decrease on T-N and unit cell volume due to the chemical pressure. The enhancement of the effective moment suggests the presence of Yb3+ while the constancy of the saturation magnetization points to a fixed 2 + valence for Eu.

Physica B-Condensed Matter 403[5-9], 946-947. 2008.

P102-08 "Evidences of the simultaneous presence of bowtie and diamond scars in rare-earth doped amorphous silicon microstadium resonators"

Figueira, D. S. L. and Frateschi, N. C.

Microdisks and microstadium resonators were fabricated on erbium doped amorphous hydrogenated silicon (a-Si: H < Er >) layers sandwiched in air and native SiO2 on Si substrates. Annealing condition is optimized to allow large emission at 1550 nm for samples with erbium concentrations as high as 1.02 x 10(20) atoms/cm(3). Near field scanning optical microscopy shows evidence of the simultaneous presence of bow-tie and diamond scars. These modes indicate the high quality of the resonators and the potentiality for achieving amorphous silicon microcavity lasers.

Journal of Applied Physics 103[6]. 063106-063106-4. 2008.

P103-08 "Factors affecting seed predation of Eriotheca gracipiles (Bombacaceae) by parakeets in a cerrado fragment"

Francisco, M. R., Lunardi, V. O., Guimaraes, P. R., and Galetti, M.

Psittacids are important pre-dispersal seed predators. However, little is known about the parameters that may determine seed predation rates by these birds, such as plants' characteristics and microhabitat. Eriotheca gracilipes (Bombacaceae) is a semi-deciduous tree widely distributed in the Brazilian cerrado. The fruits are dehiscent pods and the seeds are winddispersed. Some individuals lose their leaves during the fruiting season, getting very conspicuous. Here we tested the hypothesis that the absence of leaves in E. gracilipes during the fruiting season may increase pre-dispersal seed predation by psittacids. We also tested the hypotheses that (1) seed predation intensity increases with increasing plant size and (2) number of fruits, (3) seed predation decreases with the increasing number of conspecific plants in a range of 15 m, and (4) seed predation intensity is lower in plants with higher vegetation cover over their crowns. The small parakeet Brotogeris versicolurus was the only species observed preying upon the seeds of E. gracilipes. The percentage of fruits damaged by the parakeets ranged from 0 to 100% (66.98 +/-43.11%, n = 72) among the different plants. Our data give weak support to the hypothesis that the absence of leaves may facilitate plants and/or fruits detection by the parakeets. However, seed predation intensity was significantly affected by crop size. The hypothesis that conspecific fruiting plants surrounding the studied individuals may reduce predation rate was not supported. Nevertheless, trees without higher vegetation cover over their crowns were significantly affected by increased seed predation. This suggests that seed predation by parakeets can be a potential selective factor influencing fruit crop sizes in E. gracilipes.

Acta Oecologica-International Journal of Ecology 33[2], 240-245. 2008.

P104-08 "Fano resonances in the conductance of quantum dots with mixed dynamics"

Mendoza, M., Schulz, P. A., Vallejos, R. O., and Lewenkopf, C. H.

We study the conductance fluctuations of an open quantum dot with underlying mixed dynamics. In addition to smooth conductance fluctuations, typical of chaotic quantum dots, we observe the occurrence of many sharp conductance peaks. Those are associated with localized states in the quantum dot and display a variety of Fano shape resonances. We show that the Fano q parameter in the presence of time-reversal symmetry is, in general, complex. We discuss the origin of the different Fano parameters and present a numerical study to support our theory

Physical Review B 77[15]. 155307. 2008.

P105-08 "First order magnetic transition and magnetoelastic effects in Sm2IrIn8"

Lora-Serrano, R., Correa, V. F., Adriano, C., Giles, C., Duque, J. G. S., Granado, E., Pagliuso, et all

We report measurements of temperature dependent heat capacity, thermal expansion and high resolution X-ray diffraction (XRD) taken on single crystals Of Sm2IrIn8 intermetallic compound. This compound belongs to the RmMnIn3m+2n family (R = rare earth, m = 1, 2, n = 0, 1 and M = Rh, Ir and Co) which includes a number of heavy fermion superconductors for R = Ce. Particularly, Sm2IrIn8 is the only member of this family to present a first order magnetic phase transition (FOMT). Both thermal expansion and heat capacity data show very pronounced sharps peaks at T-N = 14.2K consistent with an FOMT. The linear thermal-expansion coefficient is anisotropic and both c-axis and basal ab plane coefficients change discontinuously at 14.2 K. This change is negative for both direction in contrast to what was found for other members of family such as Ce2RhIn8 and CeRhIn5. The zero-field high resolution XRD data at 14.2 K shows no evidence for a tetragonalto-orthorhombic structural phase transition. We discuss our results considering tetragonal crystalline field effects (CEF), quadupolar interactions, antiferromagnetic domains and magnetoelastic effects.

Physica B-Condensed Matter 403[5-9], 1365-1367. 2008.

P106-08 "Forward scattering approximation and bosonization in integer quantum Hall systems"

da Costa, M. R., Westfahl, H., and Caldeira, A. O.

In this work, we present a model and a method to study integer quantum Hall (IQH) systems. Making use of the Landau levels structure we divide these two-dimensional systems into a set of interacting one-dimensional gases, one for each guiding center. We show that the so-called strong field approximation, used by Kallin and Halperin and by MacDonald, is equivalent, in first order, to a forward scattering approximation and analyze the IQH systems within this approximation. Using an appropriate variation of the Landau level bosonization method we obtain the dispersion relations for the collective excitations and the single-particle spectral functions. For the bulk states, these results evidence a behavior typical of non-normal strongly correlated systems, including the spin-charge splitting of the single-particle spectral function. We discuss the origin of this behavior in the light of the Tomonaga-Luttinger model and the bosonization of two-dimensional electron gases.

Annals of Physics 323[3], 673-704. 2008.

P107-08 "Influence of Ge on magnetic and structural propertiesof Joule-heated Co-based ribbons: Giant magnetoimpedance response"

Muraca, D., Cremaschi, V., Knobel, M., and Sirkin, H.

Studies of magnetic and structural properties of Fe3.5Co66.5Si12-xGexB18 (x = 0, 3, and 6) soft magnetic ribbons obtained by melt-spinning were performed. The samples were submitted to Joule-heating treatments with different maximum current values (0.01, 0.05, 0.1, 0.2, and 0.8 A, respectively) with steps of 0.01A and times by step of 1, 2, and 10s). X-ray diffraction, temperature dependence of magnetization (for the as-quenched samples), coercivity and giant magnetoimpedance (GMI), measured at different frequencies (100, 500, and 900 kHz, respectively) were performed. All the samples crystallized at annealing currents higher than 0.4 A, which was consistent with the magnetic hardening of the material. Coercivities less than 1 A/m were obtained for the three samples between 0.1 and 0.2 A. Maximum value of GMI response was observed for the sample without Ge in the as-quenched state.

Journal of Magnetism and Magnetic Materials 320[15], 2068-2073. 2008.

P108-08 "Low-energy elastic scattering of positrons by N2O"

Arretche, F., Mazon, K. T., Michelin, S. E., Lee, M. T., and Lima, M. A. P.

We present a theoretical investigation on positron scattering by N2O. Elastic differential and integral cross sections at both the static and static plus correlation-polarization levels of approximation are calculated and reported in the 0.1-100 eV. Calculations were performed using two theoretical methods, namely, the Schwinger multichannel method and the method of continued fractions. Also, two different schemes were used to treat correlation-polarization effects. The comparison between our calculated results and the existing experimental data is encouraging.

Physical Review A 77[4]. 042708. 2008.

P109-08 "Low-energy electron scattering from methanol and ethanol"

Khakoo, M. A., Blumer, J., Keane, K., Campbell, C., Silva, H., Lopes, M. C. A., Winstead, C., Mckoy, V., da Costa, R. F., Ferreira, L. G., Lima, M. A. P., and Bettega, M. H. F.

Measured and calculated differential cross sections for elastic (rotationally unresolved) electron scattering from two primary alcohols, methanol (CH3OH) and ethanol (C2H5OH), are reported. The measurements are obtained using the relative flow method with helium as the standard gas and a thin aperture as the collimating target gas source. The relative flow method is applied without the restriction imposed by the relative flow pressure conditions on helium and the unknown gas. The experimental data were taken at incident electron energies of 1, 2, 5, 10, 15, 20, 30, 50, and 100 eV and for scattering angles of 5 degrees-130 degrees. There are no previous reports of experimental electron scattering differential cross sections for CH3OH and C2H5OH in the literature. The calculated differential cross sections are obtained using two different implementations of the Schwinger multichannel method, one that takes all electrons into account and is adapted for parallel computers, and another that uses pseudopotentials and considers only the valence electrons. Comparison between theory and experiment shows that theory is able to describe low-energy electron scattering from these polyatomic targets quite well

Physical Review A 77[4]. 042705. 2008.

P110-08 "Magnetic and magnetocaloric properties on the U1-yRyGa2 (R=Er and Dy) compound"

da Silva, L. M., dos Santos, A. O., Gandra, F. G., Cardoso, L. P., and Gama, S.

The magnetic, calorimetric, and magnetocaloric properties of the pseudobinary U1-yRyGa2 (R=Er and Dy) series were studied to determine its potential as a candidate for use in cryogenic magnetic refrigeration. The partial substitution of Dy and Er for U provides a wide range of the ordering temperature and increases the saturation magnetic moment. The results for U1--yDyyGa2 with 0.6 < y < 0.9 show evidences of a spin-glass-like (SG) behavior, possibly as a consequence of competing anisotropy and exchange interactions within a frustrated hexagonal spin lattice. The isothermal magnetic entropy change (Delta S-mag) observed for UGa2 shows a well defined peak centered on T-C, which is gradually broadened and shifted to lower temperatures as the Er and Dy content increases. For low concentrations (0.2 <= y <= 0.4) a tablelike profile is observed in the Delta S-mag curve.

Journal of Applied Physics 103[7]. 07B308-07B308-3. 2008.

P111-08 "Magnetic properties of one-dimensional CoCu(opba) systems and DFT studies of the building blocks"

Pedroso, E. F., Pereira, C. L. M., dos Santos, H. F., de Oliveira, L. F. C., Nunes, W. C., Knobel, M., and Stumpf, H. O.

The synthesis of one-dimensional, molecule-based magnets and the investigation of their structure and physical properties are described. The one-dimensional CoCu(opba) system, where opba [orthophenylenebis(oxamato)] bridges the metal ions resulted in antiferromagnetic coupling, and was studied by insertion of electron donating and electron withdrawing groups in the organic ligands' aromatic rings. In order to verify the influence of these modi. cations, three compounds of the formula [CoCu(opba-xy)], where x = y = CH3 (compound 1), x = y = Cl (compound 2), x = H and y = NO2 (compound 3) are described. The electronic structure of the oxamato bridge group has been studied using calculations at the density functional heory (DFT) level for [Cu(opba-xy)](2)-building blocks. Magnetic measurements in polycrystalline samples showed ferrimagnetic behavior for the three compounds. Least-squares fits of the experimental data indicate antiferromagnetic couplings J(CoCu) of -35.0, -32.9 and - 24.2 cm(-1) for 1, 2 and 3, respectively.

Journal of Magnetism and Magnetic Materials 320[14], E200--E203. 2008.

P112-08 "Magnetic properties of nanocrystalline CoFe2O4 synthesized by modified citrate-gel method"

Turtelli, R. S., Duong, G. V., Nunes, W., Grossinger, R., and Knobel, M.

Nanocrystalline CoFe2O4 with an average grain size of about 40nm was successfully prepared by a modified citrate-gel method. At temperatures of 3 and 300 K, the measured coercive fields are 0.43 and 0.07T and the magnetizations at 7T are 89 and 83 emu/g, respectively. At room temperature, the longitudinal and transversal magnetostriction values are -130 and 70 ppm, respectively. The contribution of a disordered magnetic phase was detected by the occurrence of a peak in the ac-susceptibilities curves at around 250 K. The temperature dependence of the field-cooled and zero fieldcooled low-field magnetization showed a larger irreversibility below this temperature. This disordered phase behaves like a spin-glass, which is coexisting with the ferrimagnetically ordered main phase.

Journal of Magnetism and Magnetic Materials 320[14], E339-E342. 2008.

P113-08 "Magnetism in Gd-W films"

Gadioli, G. Z., Rouxinol, F. P., Gelamo, R. V., dos Santos, A. O., Cardoso, L. P., and de Moraes, M. A. B.

Vapor condensation techniques are useful to prepare magnetic alloys whose components have low or even negligible equilibrium mutual solubility. In this work, one of these techniques-sputtering-was used to obtain GdxW1-x alloys whose magnetic properties were investigated as a function of the Gd atomic concentration x. Gadolinium and various Gd-based alloys are promising materials for magnetic refrigeration and this was one of the motivations for this study. The Gd-x-W1-x films were sputter deposited from Gd and W targets with x ranging from 0 to 1 as determined by x-ray energy-dispersive spectroscopic analyses. X-ray diffraction patterns indicate that crystalline structures were formed at low and high Gd concentrations, while at intermediate concentrations, the films were amorphous. Magnetization measurements, performed as a function of temperature and with static and alternating applied fields, reveal a spin glasslike behavior in all the W-containing samples for temperatures below the freezing temperature T-f. For low and intermediate Gd concentrations, and for T>T-f, the films were paramagnetic, while a ferromagnetic phase was observed in the Gd-W alloy of the highest Gd content. The magnetocaloric effect was investigated from the magnetization isotherms M versus H, from which the isothermal magnetic entropy variation Delta S-M as a function of T, for the removal of an applied field of 50 kOe, was determined. It was observed that the maximum value of Delta S-M for each Delta S-M versus T curve and the temperature at which these maxima occur, are strongly dependent on x.

Journal of Applied Physics 103[9]. 093916. 2008.

P114-08 "Magnetoelastic and thermal effects in the BiMn2O5lattice: A high-resolution x-ray diffraction study"

Granado, E., Eleoterio, M. S., Garcia-Flores, A. F., Souza, J. A., Golovenchits, E. I., and Sanina, V. A.

High-resolution synchrotron x-ray diffraction measurements were performed on single crystalline and powder samples of BiMn2O5. A linear temperature dependence of the unit cell volume was found between T-N=38 and 100 K, suggesting that a low-energy lattice excitation may be responsible for the lattice expansion in this temperature range. Between T-*similar to 65 K and T-N, all lattice parameters showed incipient magnetoelastic effects, due to shortrange spin correlations. An anisotropic strain along the a direction was also observed below T-*. Below T-N, a relatively large contraction of the a parameter following the square of the average sublattice magnetization of Mn was found, indicating that a second-order spin Hamiltonian accounts for the magnetic interactions along this direction. On the other hand, the more complex behaviors found for b and c suggest additional magnetic transitions below T-N and perhaps higher-order terms in the spin Hamiltonian. Polycrystalline samples grown by distinct routes and with nearly homogeneous crystal structure above T-N presented structural phase coexistence below T-N, indicating a close competition amongst distinct magnetostructural states in this compound.

Physical Review B 77[13]. 134101. 2008.

P115-08 "Measuring electrical and mechanical properties of red blood cells with double optical tweezers"

Fontes, A., Fernandes, H. P., De Thomaz, A. A., Barbosa, L. C., Barjas-Castro, M. L., and Cesar, C. L.

Red blood cell (RBC) aggregation in the blood stream is prevented by the zeta potential created by its negatively charged membrane. There are techniques, however, to decrease the zeta potential and allow cell agglutination, which are the basis of most of antigen-antibody tests used in immunohematology. We propose the use of optical tweezers to measure membrane viscosity, adhesion, zeta potential, and the double layer thickness of charges (DLT) formed around the cell in an electrolytic solution. For the membrane viscosity experiment, we trap a bead attached to RBCs and measure the force to slide one RBC over the other as a function of the velocity. Adhesion is quantified by displacing two RBCs apart until disagglutination. The DLT is measured using the force on the bead attached to a single RBC in response to an applied voltage. The zeta potential is obtained by measuring the terminal velocity after releasing the RBC from the trap at the last applied voltage. We believe that the methodology proposed here can provide information about agglutination, help to improve the tests usually performed in transfusion services, and be applied for zeta potential measurements in other samples.

Journal of Biomedical Optics 13[1]. 014001. 2008.

P116-08 "Meldola blue immobilized on a new SiO2/TiO2/graphite composite for electrocatalytic oxidation of NADH"

Maroneze, C. M., Arenas, L. T., Luz, R. C. S., Benvenutti, E. V., Landers, R., and Gushikem, Y.

Meldola blue immobilized on a new SiO2/TiO2/graphite composite was applied in the electrocatalytic oxidation of NADH. The materials were prepared by the sol-gel processing method and characterized by several techniques including scanning electronic microscopy coupled to energy dispersive spectroscopy (SEM-EDS), X-ray photoelectron spectroscopy (XPS) and high-resolution transmission electronic microscopy (HRTEM). Si and Ti mapping profiles Oil the surface showed a homogeneous distribution of the components. Ti2p binding energy peaks indicate that the formation of Si-O-Ti linkage is presumably the responsible for the high rigidity of the matrices. The good electrical conductivity presented by the composites (5 and 11S cm(-1)) can be related to a homogeneous distribution of graphite particles observed by TEM. After the materials characterization, a SiO2/TiO2/graphite electrode was prepared and some chemical modifications were performed on its surface to promote the adsorption of meldola blue. The resulting system presented electrocatalytic properties toward the oxidation of NADH, decreasing the oxidation potential to -120 mV. The proposed sensor showed a wide linear response range from 0.018 to 7.29 mmol l(-1) and limit of detection of 0.008 mmol l(-1). SiO2/TiO2/graphite has shown to he a promising material to be used asa suitable support in the construction of new electrochemical sensors.

Electrochimica Acta 53[12], 4167-4175. 2008.

P117-08 "Mobius and twisted graphene nanoribbons: Stability, geometry, and electronic properties"

Caetano, E. W. S., Freire, V. N., dos Santos, S. G., Galvao, D. S., and Sato, F.

Results of classical force field geometry optimizations for twisted graphene nanoribbons with a number of twists N-t varying from 0 to 7 (the case N-t=1 corresponds to a half-twist Mobius nanoribbon) are presented in this work. Their structural stability was investigated using the Brenner reactive force field. The best classical molecular geometries were used as input for semiempirical calculations, from which the electronic properties were computed for each structure. CI wavefunctions were also calculated in the complete active space framework taking into account eigenstates from HOMO-4 to LUMO+4, as well as the oscillator strengths corresponding to the first optical transitions in the UV-VIS range. The lowest energy molecules were found less symmetric than initial configurations, and the HOMO-LUMO energy gaps are larger than the value found for the nanographene used to build them due to electronic localization effects created by the twisting. A high number of twists leads to a sharp increase of the HOMO -> LUMO transition energy. We suggest that some twisted nanoribbons could form crystals stabilized by dipolar interactions.

Journal of Chemical Physics 128[16]. 164719-164719-8. 2008.

P118-08 "Modeling equilibrium concentrations of Bjerrum and molecular point defects and their complexes in ice I-h"

de Koning, M. and Antonelli, A.

We present a model for the determination of the thermal equilibrium concentrations of Bjerrum defects, molecular point defects, and their aggregates in ice I-h. First, using a procedure which minimizes the free energy of an ice crystal with respect to the numbers of defect species, we derive a set of equations for the equilibrium concentrations of free Bjerrum and point defects, as well their complexes. Using density-functional-theory calculations, we then evaluate the binding energies of Bjerrum-defect/vacancy and Bjerrumdefect/interstitial complexes. In contrast to the complexes which involve the molecular vacancy, the results suggest that the molecular interstitial binds preferentially to the D-type Bjerrum defect. Using both theoretical binding and formation free energies as well as the available experimental data, we find that the preferential binding and the substantial presence of the interstitial as the predominant point defect in ice I-h may lead to conditions in which the number of free D defects becomes considerably smaller than that of free L defects. Such a scenario could possibly be involved in the experimentally observed inactivity of D-type Bjerrum defects in the electrical properties of ice I-h. **Journal of Chemical Physics 128[16]. 164502. 2008.**

P119-08 "Multistep ionization of argon clusters in intense femtosecond extreme ultraviolet pulses"

Bostedt, C., Thomas, H., Hoener, M., Eremina, E., Fennel, T., Meiwes-Broer, K. H., Wabnitz, H., Kuhlmann, M., Ploenjes, E., Tiedtke, K., Treusch, R., Feldhaus, J., de Castro, A. R. B., and Moller, T.

The interaction of intense extreme ultraviolet femtosecond laser pulses (lambda=32.8 nm) from the FLASH free electron laser (FEL) with clusters has been investigated by means of photoelectron spectroscopy and modeled by Monte Carlo simulations. For laser intensities up to 5x10(13) W/cm(2), we find that the cluster ionization process is a sequence of direct electron emission events in a developing Coulomb field. A nanoplasma is formed only at the highest investigated power densities where ionization is frustrated due to the deep cluster potential. In contrast with earlier studies in the IR and vacuum ultraviolet spectral regime, we find no evidence for electron emission from plasma heating processes.

Physical Review Letters 100[13]. 133401. 2008.

P120-08 "Nanotexturized polytetrafluoroethylene substrates formed by large crystalline nanofibrils in amorphous matrices"

de Souza, E. F., Torriani, I. C. L., and Teschke, O.

Plastic deformation has proved to be an attractive tool for obtaining ultrafine grained and nanocrystalline metallic materials. A description of plastic deformation as a technique to create nanotexturized polytetrafluoroethylene substrates free of defects, such as pores or impurities, which has potential applications as templates for the oriented growth of organic and inorganic compounds, is presented here. The obtained morphology characterized by nanosized fibrils arrangements was revealed by atomic force microscopy. Nanofibrils with a width from 330 to 980 nm and lengths from 1.85 to 11 mu m were observed on polytetrafluoroethylene substrates annealed at 330 degrees C and 390 degrees C, respectively. Wide angle X-ray scattering spectra for untreated and annealed samples show that there is a slight decrease in the amorphous component for samples annealed at 380 degrees C but not for samples annealed at 330 degrees C showing that the amorphous substrate matrix in little altered by the annealing. The pattern formation is associated with superficial polymeric domains that become large crystalline nanofibrils in an amorphous matrix.

Journal of Nanoscience and Nanotechnology 8[4], 2135-2142. 2008.

P121-08 "Near threshold vibrational excitation of molecules by positron impact: A projection operator approach"

Varella, M. T. D., de Oliveira, E. M., and Lima, M. A. P.

We report vibrational excitation (v(i) = 0 -> v(f) = 1) cross-sections for positron scattering by H-2 and model calculations for the (v(i) = 0 -> v(f) = 1) excitation of the C-C symmetric stretch mode of C2H2. The Feshbach projection operator formalism was employed to vibrationally resolve the fixed-nuclei phase shifts obtained with the Schwinger multichannel method. The near threshold behavior of H-2 and C2H2 significantly differ in the sense that no low lying singularity (either virtual or bound state) was found for the former, while a e(+)-acetylene virtual state was found at the equilibrium geometry (this virtual state becomes a bound state upon stretching the molecule). For C2H2, we also performed model calculations comparing excitation cross-sections arising from virtual (-i kappa(0)) and bound (+i kappa(0)) states symmetrically located around the origin of the complex momentum plane (i.e. having the same kappa(0)). The virtual state is seen to significantly couple to vibrations, and similar crosssections were obtained for shallow bound and virtual states.

Nuclear Instruments & Methods in Physics Research Section BBeam Interactions with Materials and Atoms 266[3], 435-440. 2008.

P122-08 "Obtaining the gauge invariant kinetic term for a SU(n)(U) circle times SU(m)(V) Lagrangian"

Bernardini, A. E.

We propose a generalized way to formally obtain the gauge invariance of the kinetic part of a field Lagrangian over which a gauge transformation ruled by an SU(n) (U) circle times SU(m) (V) coupling symmetry is applied. As an illustrative example, we employ such a formal construction for reproducing the standard model Lagrangian. This generalized formulation is supposed to contribute for initiating the study of gauge transformation applied to generalized SU(n) (U) circle times SU(m) (V) symmetries as well as for complementing an introductory study of the standard model of elementary particles.

International Journal of Theoretical Physics 47[4], 971-976. 2008.

P123-08 "Physical parameters and basis transformations in the two-Higgs-doublet model"

Nishi, C. C.

A direct connection between physical parameters of general two-Higgs-doublet model (2HDM) potentials after electroweak symmetry breaking (EWSB) and the parameters that define the potentials before EWSB is established. These physical parameters, such as the mass matrix of the neutral Higgs bosons, have well-defined transformation properties under basis transformations transposed to the fields after EWSB. The relations are also explicitly written in a basis covariant form. Violation of these relations may indicate models beyond 2HDMs. In certain cases the whole potential can be defined in terms of the physical parameters. The distinction between basis transformations and reparametrizations is pointed out. Some physical implications are discussed.

Physical Review D 77[5]. 055009. 2008.

P124-08 "Physical properties of disordered double-perovskite Ca2-xLaxFeIrO6"

Bufaical, L., Ferreira, L. M., Lora-Serrano, R., Aguero, O., Torriani, I., Granado, E., Pagliuso, P. G., Caytuero, A., and Baggio-Saitovich, E.

In this work we have synthesized polycrystalline samples for the series of double-perovskite Ca2-xLaxFeIrO6. Their structural and magnetic properties were investigated using experiments of magnetic susceptibility and x-ray powder diffraction. The Ca2-xLaxFeIrO6 compounds form in a monoclinic structure, space group P21/n, with the presence of significant Fe/Ir cationic disorder. Interestingly, our results indicate a change in the nature of the microscopic magnetic interaction induced by La doping, where the system seems to evolve from antiferromagnetic in the extremities of the series, x=0 (T-N approximate to 75 K) and x=2.0, to ferrimagnetic in intermediate regions of the series. However, due to significant presence of disorder and strong competition between ferromagnetic and antiferromagnetic interactions, the saturation of the magnetization was not found to be larger than 0.1 mu(B)/Fe.

Journal of Applied Physics 103[7]. 07F716-07F716-3. 2008.

P125-08 "Polarization effects on electronic excitation of the (a)over-tilde(3)B(1u) state of ethylene by low-energy electron impact"

da Costa, R. F., Bettega, M. H. F., and Lima, M. A. P.

In this work, we investigated the influence of polarization effects on the electronic excitation of the a B-3(1u) state of ethylene. We employed the Schwinger multichannel method implemented with pseudopotentials to compute the elastic and the inelastic scattering cross sections for energies between 0 and 8 eV. Elastic calculations were performed in the static-exchange and static-exchange plus polarization approximations, and inelastic calculations were performed in a two-channel approximation with and without the inclusion of polarization effects. The scattering amplitudes are generated in the scope of the minimal orbital basis for single configuration interactions strategy. Ethylene presents a shape resonance in the B-2(2g) symmetry located close to the threshold of the a B-3(1u) state. We show that the inclusion of polarization effects has a great influence on the excitation cross section and also that, in this case, just the two-channel close coupling without polarization is not enough to provide reliable results. In particular, our computed inelastic differential cross sections obtained with the proper treatment of polarization are in better agreement with the experimental values. They are smaller in magnitude than those obtained in the two-channel calculation without the inclusion of polarization effects. These results confirm our expectations reported in a recent publication on electron collisions with furan

Physical Review A 77[4]. 042723. 2008.

P126-08 "Polarization resolved luminescence in asymmetric n-type GaAs/AlGaAs resonant tunneling diodes"

dos Santos, L. F., Gobato, Y. G., Lopez-Richard, V., Marques, G. E., Brasil, M. J. S. P., Henini, M., and Airey, R. J.

We have investigated the polarized emission from a n-type GaAs/AlGaAs resonant tunneling diode under magnetic field. The GaAs contact layer emission shows a large constant negative circular polarization. A similar result is observed for the quantum well, but only when electrons are injected from the substrate, while for inverted biases, the polarization tends to become positive for small voltages and large laser excitation intensities. We believe that the quantum well polarization may be associated to the partial thermalization of minority carriers on the well subbands and is thus critically dependent on the bias-controlled density of carriers accumulated in the well.

Applied Physics Letters 92[14]. 143505. 2008.

P127-08 "Probing the structure of nanograined CuO powders"

Bianchi, A. E., Plivelic, T. S., Punte, G., and Torriani, I. L.

The microstructural properties of polycrystalline CuO powders and their evolution during controlled high energetic ball milling (HEBM) were studied using conventional X-ray diffraction (XRD) techniques and in situ temperature-dependent small and wide angle scattering (SAXS-WAXS) synchrotron radiation experiments. Volume weighted average grain size, unit cell expansion, oxygen deficiency, and microstrain values as a function of milling time were obtained from XRD. SAXS data revealed different nanostructures for samples synthesized by one-step solid-state reaction (SSR) or HEBM-treated powders. The latter presented the characteristics of a multilayered nanoscale solid system with surface fractal behavior. Correlation of the XRD microstructural parameters and the power law exponent of the SAXS curves as a function of temperature and milling time provided a coherent picture of the structure of HEBM-treated powders. The overall structural information presented in this article may shed some light on the macroscopic physical properties of CuO nanostructures

Journal of Materials Science 43[10], 3704-3712. 2008.

P128-08 "Projected-length distributions of fission-fragment tracks from U and Th thin film sources in muscovite"

Guedes, S., Jonckheere, R., Iunes, P. J., and Hadler, J. C.

Thin films of natural uranium and thorium deposited on muscovite were used as sources of neutron-induced fission fragments. Fragment energy loss in thin-source geometry is negligible. In this way, the observed fragment range results from the interaction of the fragment with the detector material. This characteristic enables the investigation of asymmetric fission and etching, through measurements of projected track length distributions in muscovite micas coupled with thin films. The means and standard deviations of the etchable length distributions of the heavy and light fission-fragment tracks were estimated by fitting a theoretical equation to the experimental data. The light fission-fragment accounts for similar to 54% and the heavy fission-fragment for similar to 46% of the etchable length of a full fission track. This average partition is the same for tracks from thermal-neutron-induced fission of U-235 and fast-neutron-induced fission of Th-232. The mean etchable length of uranium fission tracks is similar to 2.5% longer than that of thorium fission tracks. This difference is at the resolution limit of these measurements but correlates with the difference in the mean combined initial kinetic energies of the fission fragments. The mean etchable length of uranium fission tracks in muscovite is similar to 5% shorter than their calculated latent track length, supporting earlier estimates of a length deficit of this magnitude. The length deficit and the standard deviation of the etchable length distribution of the light fission-fragment tracks are twice the equivalent values for the heavy fissionfragment tracks. This is interpreted in terms of a upsilon(t)-profile (track etch rate) that depends on the mass of the track-forming particle.

Nuclear Instruments & Methods in Physics Research Section B Beam Interactions with Materials and Atoms 266[5], 786-790. 2008.

P129-08 "Quantum-classical correspondence in the phase control of multiphoton dissociation by two-color laser pulses"

de Lima, E. F. and de Aguiar, M. A. M.

The quantum and the classical multiphoton dissociation dynamics of diatomic Morse molecules driven by intense and ultrashort two-color laser pulses are investigated and compared. Special attention is given to the role of the relative phase of the monochromatic components of the pulses. We study the excitation of the system from the vibrational ground state and from excited states for several values of amplitude, frequency, and duration of the external pulses. Similar overall sensitivity of the dissociation threshold on the phase is observed in both quantum and classical approaches, provided the excitation frequency is sufficiently far from quantum resonances. In addition, we analyze the correspondence between the effects of the relative phase on the classical and quantum dynamics.

Physical Review A 77[3]. 033406. 2008.

P130-08 "Rabi oscillation damping of two-level states in quantum dots"

Mogilevtsev, D., Nisovtsev, A. P., Kilin, S., Cavalcanti, S. B., Brandi, H. S., and Oliveira, L. E.

Within a general approach suitable to describe a coherently driven two-level system interacting with a dephasing reservoir, we have proposed various mechanisms to explain the nature of the damping of Rabi oscillations with increasing drivingpulse area in localized two-level semiconductor systems. We have shown that the non-Markovian character of the reservoir leads to the dependence of the dephasing rate on the drivingfield intensity, as observed experimentally. Furthermore, we have also shown that stationary as well as non-stationary effects resulting from the coupling to the environment may give rise to intensity-dependent damping of oscillations.

Physica E-Low-Dimensional Systems & Nanostructures 40[5], 1487-1489. 2008.

P131-08 "rho(0) photoproduction in ultraperipheral relativistic heavy ion collisions at root s(NN)=200 GeV"

Abelev, B. I., Aggarwal, M. M., Ahammed, Z., Anderson, B. D., Arkhipkin, D., Averichev, G. S., Bai, Y., et all

Photoproduction reactions occur when the electromagnetic field of a relativistic heavy ion interacts with another heavy ion. The STAR Collaboration presents a measurement of rho(0) and direct pi(+)pi(-) photoproduction in ultraperipheral relativistic heavy ion collisions at root s(NN) = 200 GeV. We observe both exclusive photoproduction and photoproduction accompanied by mutual Coulomb excitation. We find a coherent cross section of sigma(AuAu -> Au*Au*rho(0)) = 530 +/- 19(stat.) +/- 57(syst.) mb, in accord with theoretical calculations based on a Glauber approach, but considerably below the predictions of a color dipole model. The rho 0 transverse momentum spectrum (p(T)(2)) is fit by a double exponential curve including both coherent and incoherent coupling to the target nucleus; we find sigma(inc)/sigma(coh) = 0.29 +/- 0.03 (stat.) +/- 0.08 (syst.). The ratio of direct pi(+)pi(-) to rho(0) production is comparable to that observed in gamma(p) collisions at HERA and appears to be independent of photon energy. Finally, the measured rho(0) spin helicity matrix elements agree within errors with the expected s-channel helicity conservation

Physical Review C 77[3]. 034910. 2008.

P132-08 "Selective and efficient excitation of diatomic molecules by an ultrashort pulse train" de Araujo, L. E. E.

In this paper, I discuss the selective and efficient vibrational population transfer between electronic states of diatomic molecules by a weak, ultrashort pulse train. The spectrum of each individual pulse in the train is wide enough to simultaneously excite several vibrational levels of the molecule. However, selectivity is achieved by mismatching the frequency comb, associated with the pulse train, to the excited vibrational levels. Efficiency results from the coherent accumulation of population from one pulse in the train to the next

Physical Review A 77[3]. 033419. 2008.

P133-08 "Sign change of Poisson's ratio for carbon nanotube sheets"

Hall, L. J., Coluci, V. R., Galvao, D. S., Kozlov, M. E., Zhang, M., Dantas, S. O., and Baughman, R. H.

Most materials shrink laterally like a rubber band when stretched, so their Poisson's ratios are positive. Likewise, most materials contract in all directions when hydrostatically compressed and decrease density when stretched, so they have positive linear compressibilities. We found that the in- plane Poisson's ratio of carbon nanotube sheets (buckypaper) can be tuned from positive to negative by mixing single- walled and multiwalled nanotubes. Density- normalized sheet toughness, strength, and modulus were substantially increased by this mixing. A simple model predicts the sign and magnitude of Poisson's ratio for buckypaper from the relative ease of nanofiber bending and stretch, and explains why the Poisson's ratios of ordinary writing paper are positive and much larger. Theory also explains why the negative in- plane Poisson's ratio is associated with a large positive Poisson's ratio for the sheet thickness, and predicts that hydrostatic compression can produce biaxial sheet expansion. This tunability of Poisson's ratio can be exploited in the design of sheet- derived composites, artificial muscles, gaskets, and chemical and mechanical sensors

Science 320[5875], 504-507. 2008.

P134-08 "Spin-orbit dependence on carrier momentum in (110) GaAs quantum wells"

Couto, O. D. D., Rudolph, J., Iikawa, F., Hey, R., and Santos, P. V.

Surface acoustic waves (SAW) are employed to transport optically generated spin ensembles over distances exceeding 60 gm in (110) GaAs quantum wells (QW). The dependence of the spin-orbit (SO) coupling on carrier momentum is investigated by using SAWs to transport spins with well-defined velocity along different directions in the QW plane. For transport along the [001] direction, the high relaxation rates for the in-plane spin component lead to fast spin decoherence under a magnetic field. For the [(1) over bar 10] direction, in contrast, a non-zero average value of the SO internal magnetic field retards the longitudinal spin relaxation.

Physica E-Low-Dimensional Systems & Nanostructures 40[6], 1797-1799. 2008.

P135-08 "Spin structure and first-order transition of GdIn3: Near-surface magnetism, buried amplitude-modulated phase, and interface delocalization"

Malachias, A., Granado, E., Lora-Serrano, R., Pagliuso, P. G., and Perez, C. A.

A resonant x-ray magnetic diffraction study was performed for pure and (Cd,Ga)-doped GdIn3 single crystals with cubic structure. All studied samples show an equal-magnitude antiferromagnetic spin structure with propagation vector (tau) over right arrow=[1/2, 1/2,0] at low temperatures, corresponding to a parallel spin propagation along the (c) over right arrow direction (normal to the studied surfaces) and antiparallel propagation along (a) over right arrow and (b) over right arrow. A complex magnetic behavior in the submicrometric near-surface region (NSR) was found close to T-N(bulk) similar to 44 K. For both pure and substituted samples, a fairly strong signal from the equal-magnitude magnetic phase was found to survive above T-N(bulk) and abruptly disappears at T-N(NSR) similar to T-N(bulk)+ 0.7 K, indicating that the NSR may show a larger T-N than the bulk for all studied samples. For the pure compound only, satellite peaks consistent with an amplitude-modulated magnetic phase with a wavelength of 380 angstrom were found between T-N(bulk) and T-N(NSR). A successful fit of the scattering profile around several magnetic Bragg positions and photon energies, using a simple phase coexistence model, confirmed that the amplitude-modulated phase develops underneath the most superficial region showing the equal magnitude structure. The evolution of the magnetic scattering profile on cooling indicates that the interface between equal-magnitude and amplitude-modulated phases diverges towards the bulk as T -> T-N(bulk) from above. A detailed analysis of the magnetic scattering, as well as the existence of a single bulk transition within the experimental sensitivity of our specific heat and magnetic susceptibility measurements, in contrast to the rich behavior shown by the near-surface region, indicates that the amplitude-modulated phase is not bulk representative, being actually sandwiched between the bulk paramagnetic and the equal-magnitude phases. Depth-temperature phase diagrams for pure and (Ga,Cd)-doped GdIn3 are drawn on the basis of our results, which are discussed in terms of a three-phase coexistence scenario theoretically proposed for first-order transitions in the NSR

Physical Review B 77[9]. 094425. 2008.

P136-08 "Structure, magnetism, and magnetocaloric properties of MnFeP1-xSix compounds"

Thanh, D. T. C., Brueck, E., Trung, N. T., Klaasse, J. C. P., Buschow, K. H. J., Ou, Z. Q., Tegus, O., and Caron, L.

MnFeP1-xSix compounds with x=0.10,0.20,0.24,0.28,...,0.80,1 were prepared by high-energy ball milling and solid-state reaction. The structural, magnetic, and magnetocaloric properties are investigated as a function of temperature and magnetic field. X-ray diffraction studies show that the samples in the range from x=0.28 to 0.64 adopt the hexagonal Fe2P-type structure with a small amount of second phase which increases with increasing Si content. The samples with lower Si content show the orthorhombic Co2P-type structure. Magnetic measurements show that the paramagnetic-ferromagnetic transition temperatures range from 214 to 377 K. Of much importance is the fact that these compounds do not contain any toxic components and exhibit excellent magnetocaloric properties.

Journal of Applied Physics 103[7]. 07B318-07B318-3. 2008.

P137-08 "Study of muon neutrino disappearance using the Fermilab Main Injector neutrino beam"

Adamson, P., Andreopoulos, C., Arms, K. E., Armstrong, R., Auty, D. J., Avvakumov, S., Ayres, D. S., Baller, B., et all

We report the results of a search for nu(mu) disappearance by the Main Injector Neutrino Oscillation Search [D. G. Michael (MINOS), Phys. Rev. Lett. 97, 191801 (2006).]. The experiment uses two detectors separated by 734 km to observe a beam of neutrinos created by the Neutrinos at the Main Injector facility at Fermi National Accelerator Laboratory. The data were collected in the first 282 days of beam operations and correspond to an exposure of 1.27x10(20) protons on target. Based on measurements in the Near Detector, in the absence of neutrino oscillations we expected 336 +/- 14 nu(mu) charged-current interactions at the Far Detector but observed 215. This deficit of events corresponds to a significance of 5.2 standard deviations. The deficit is energy dependent and is consistent with two-flavor neutrino oscillations according to |Delta m(2)|=2.74(-0.26)(+0.44) x 10(-3) eV(2)/c(4) and sin(2)2 theta > 0.87 at 68% confidence level

Physical Review D 77[7]. 072002. 2008.

P138-08 "Study of the magnetic properties on Mn and As co-implanted GaAs"

De Biasi, E., Pudenzi, M. A. A., Behar, M., Carvasan, F., and Knobel, M.

The interest on diluted magnetic semiconductor (DMS), like GaMnAs, has increased during the last years due to potential applications, mainly on spintronic device. The magnetic anisotropy and the interacting effects between the magnetic nanostructures are fundamental topics to be studied. In this work we present some results on Mn and As co-implanted GaAs. Samples with three different implantation energies of Mn were prepared, keeping the As implantation energy fixed and the Mn and As dose of 2 x 10(16) cm(-2). Annealing was done using rapid thermal annealing (RTA) at 750 degrees C for 20 and 50 s. Using a superconducting quantum interference device (SQUID) and magnetic anisotropy values reported in the literature, we have obtained information about nanocluster size distribution. Our studies indicated that the nanocluster size distribution depends on the implantation parameters and the annealing time. Differently from previous studies reported in similar samples, we have observed room-temperature hysteresis in all samples, with coercive field values typical of nanoparticle systems.

Journal of Magnetism and Magnetic Materials 320[14], E404-E407. 2008.

P139-08 "Symmetry-breaking effects upon bipartite and multipartite entanglement in the XY model"

de Oliveira, T. R., Rigolin, G., de Oliveira, M. C., and Miranda, E.

We analyze the bipartite and multipartite entanglement for the ground state of the one-dimensional XY model in a transverse magnetic field in the thermodynamical limit. We explicitly take into account the spontaneous symmetry breaking in order to explore the relation between entanglement and quantum phase transitions. As a result we show that while both bipartite and multipartite entanglement can be enhanced by spontaneous symmetry breaking deep into the ferromagnetic phase, only the latter is affected by it in the vicinity of the critical point. This result adds to the evidence that multipartite, and not bipartite, entanglement is the fundamental indicator of long-range correlations in quantum phase transitions

Physical Review A 77[3]. 032325. 2008.

P140-08 "Synthesis and characterization of NiMn2O4 nanoparticles using gelatin as organic precursor"

Almeida, J. M. A., Meneses, C. T., de Menezes, A. S., Jardim, R. F., and Sasaki, J. M.

Nanoparticles of NiMn2O4 were successfully obtained by mixing gelatin and inorganic salts NiCl2 center dot 6H(2) O and MnCl2 center dot 4H(2)O in aqueous solution. The mixture has been synthesized at different temperatures and resulted in NiMn2O4 nanoparticles with crystallites size in the range of 14-44 nm, as inferred from X-ray powder diffraction (XRPD) data. We have also observed that both the average crystallite size and the unit cell parameters increase with increasing synthesis temperature. Magnetic measurements confirmed the presence of a magnetic transition near 110K.

Journal of Magnetism and Magnetic Materials 320[14], E304-E307. 2008.

P141-08 "The electron g factor of cylindrical GaAs-Ga1-xAlxAs quantum well wires under magnetic fields applied along the wire axis"

Lopez, F. E., Rodriguez, B. A., Reyes-Gomez, E., and Oliveira, L. E.

The effects of confinement and magnetic fields on the effective electron Lande g factor of GaAs-Ga1-xAlxAs cylindrical quantum well wires are studied. Calculations were carried out via the Ogg-McCombe effective Hamiltonian which is used to describe the non-parabolicity and anisotropy effects on the electron states in the conduction band. The applied magnetic field is taken along the wire axis, and the Schrodinger equation corresponding to electron spin projections parallel and antiparallel to the magnetic field is solved by using an expansion of the electron wavefunctions in terms of two-dimensional harmonic oscillator wavefunctions Calculations for the electron g(parallel to) factor in GaAs-Ga1-xAlxAs cylindrical quantum well wires are compared with results from previous theoretical work. Moreover, the present results clearly indicate the importance of taking into account the non-parabolicity/anisotropy of the conduction band if one is interested in a quantitative understanding of the electron g factor in GaAs-Ga1-xAlxAs quantum well wires

Journal of Physics-Condensed Matter 20[17]. 175204. 2008.

P142-08 "The influence of f-type function in positron-He/ positron-H-2 scattering with the Schwinger multichannel method"

Sanchez, S. D. and Lima, M. A. P.

In this paper we present results for positron-Helium and positron-H-2 scattering with the inclusion of the f-type Cartesian Gaussian functions in our computer codes of the Schwinger multichannel method (SMC). The effects of this modification call be noticed in the integral cross-section for both studied targets, with our new curves being closer to the most recent experimental measurements. The inclusion of the f-type function in the scattering wave function expansion also helped us to obtain a better set of results with the SMC method for the annihilation parameter. Data for differential cross-section (DCS) for helium is presented as well as our improvement ill the DCS data ill the forward scattering angles for the hydrogen molecule.

Nuclear Instruments & Methods in Physics Research Section B-Beam Interactions with Materials and Atoms 266[3], 447-451. 2008.

P143-08 "The metal-insulator transition in the paramagnetic Hubbard Model" Miranda, E., Garcia, D. J., Hallberg, K., and Rozenberg, M. J.

We study the Mott transition in the Hubbard Model within the dynamical mean field theory (DMFT) approach. The DMFT equations are solved using the density matrix renormalization group technique. The densities of states for the half-filled and heavily doped cases are shown. The full phase diagram is also presented.

Physica B-Condensed Matter 403[5-9], 1465-1467. 2008.

P144-08 "Theoretical investigation on the anisotropic magnetocaloric effect: Application to DyAl2"

Von Ranke, P. J., De Oliveira, N. A., De Sousa, V. S. R., Carvalho, A. M. G., Gama, S., and Reis, M. S.

Using a simple model Hamiltonian, the formulation of the anisotropic MCE was introduced and the calculations performed for DyAl2 leads to quantitative values of Delta S-iso[0 0 1][1 0 0]. An anomalous MCE was also predicted when the magnetic. field is applied along the non-easy magnetization direction [0 0 1].

Journal of Magnetism and Magnetic Materials 320[14], E143-E146. 2008.

P145-08 "Two superconducting phases in the bi-layered alloys Ce2Rh1-xIrxIn8"

Hering, E. N., Borges, H. A., Ramos, S. M., Fontes, N. B., Baggio-Saitovich, E., Bittar, E. M., Ferreira, L. M., Lora-Serrano, R., Adriano, C., Pagliuso, P. G., Sarrao, J. L., and Thompson, J. D.

We report pressure and temperature dependent electrical resistivity measurements in the Ce2Rb1-xIrxIn8 alloys. Our results revealed two phases with zero resistance. One of these phases is induced by pressure, occurring for a range of compositions situated near the Rh-rich extreme, consistent with the behavior observed for the pure Ce2Rh1-xIrxIn5 compound. The second transition occurs for intermediate concentrations (x similar to 0.5-0.7), and in sharp contrast with the first transition, is progressively eliminated by the application of pressure. We compare the findings in the Ce2Rb1-xIrxIn8 alloys to its related Ce2Rh1-xIrxIn5, discussing how the occurrence of the superconducting phases may become unfavorable for the bi-layer alloys due to higher dimensionality and stronger disorder.

Physica B-Condensed Matter 403[5-9], 780-782. 2008.

Abstracta

Instituto de Física
Diretor: Prof. Dr. Júlio César Hadler Neto
Universidade Estadual de Campinas - UNICAMP
Cidade Universitária Zeferino Vaz
13083-859 - Campinas - SP - Brasil
e-mail: secdir@ifi.unicamp.br
Fone: 0XX 19 3521-5300

Publicação

Biblioteca do Instituto de Física Gleb Wataghin
http://webbif.ifi.unicamp.br
Diretora Técnica: Rita Aparecida Sponchiado

Elaboração
Antonela Carvalho Ribeiro
antonela@ifi.unicamp.br

Projeto Gráfico
ÍgneaDesign

Impressão

Gráfica Central - Unicamp